5-13-2020

Influence of the Spatial Distribution of Cationic Functional Groups at Nanoparticle Surfaces on Bacterial Viability and Membrane Interactions

Yongqian Zhang

Natalie V. Hudson-Smith

Seth D. Frand

Meghan S. Cahill

Larissa S. Davis

See next page for additional authors

Authors

Yongqian Zhang, Natalie V. Hudson-Smith, Seth D. Frand, Meghan S. Cahill, Larissa S. Davis, Vivian Feng, Christy L. Haynes, and Robert J. Hamers

JACS
JOURNAL OF THE AMERICAN CHEMICAL SOCIETY
pubs.acs.org/JACS
Article

Influence of the Spatial Distribution of Cationic Functional Groups at Nanoparticle Surfaces on Bacterial Viability and Membrane Interactions

Yongqian Zhang, Natalie V. Hudson-Smith, Seth D. Frand, Meghan S. Cahill, Larissa S. Davis, Z. Vivian Feng, Christy L. Haynes, and Robert J. Hamers*

Cite This: J. Am. Chem. Soc. 2020, 142, 10814−10823

ABSTRACT: While positively charged nanomaterials induce cytotoxicity in many organisms, much less is known about how the spatial distribution and presentation of molecular surface charge impact nanoparticle−biological interactions. We systematically functionalized diamond nanoparticle surfaces with five different cationic surface molecules having different molecular structures and conformations, including four small ligands and one polymer, and we then probed the molecular-level interaction between these nanoparticles and bacterial cells. *Shewanella oneidensis* MR-1 was used as a model bacterial cell system to investigate how the molecular length and conformation of cationic surface charges influence their interactions with the Gram-negative bacterial membranes. Nuclear magnetic resonance (NMR) and X-ray photoelectron spectroscopy (XPS) demonstrate the covalent modification of the nanoparticle surface with the desired cationic organic monolayers. Surprisingly, bacterial growth-based viability (GBV) and membrane damage assays both show only minimal biological impact by the NPs functionalized with short cationic ligands within the concentration range tested, yet NPs covalently linked to a cationic polymer induce strong cytotoxicity, including reduced cellular viability and significant membrane damage at the same concentration of cationic groups. Transmission electron microscopy (TEM) images of these NP-exposed bacterial cells show that NPs functionalized with cationic polymers induce significant membrane distortion and the production of outer membrane vesicle-like features, while NPs bearing short cationic ligands only exhibit weak membrane association. Our results demonstrate that the spatial distribution of molecular charge plays a key role in controlling the interaction of cationic nanoparticles with bacterial cell membranes and the subsequent biological impact. Nanoparticles functionalized with ligands having different lengths and conformations can have large differences in interactions even while having nearly identical zeta potentials. While the zeta potential is a convenient and commonly used measure of nanoparticle charge, it does not capture essential differences in molecular-level nanoparticle properties that control their biological impact.

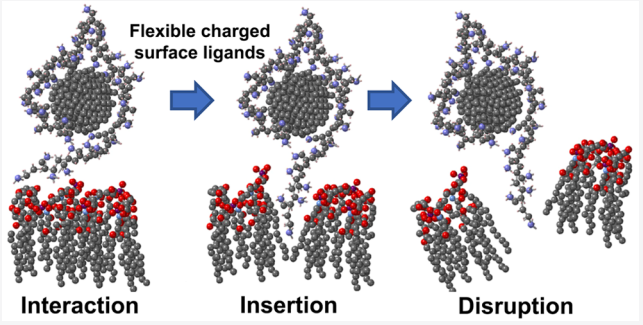

INTRODUCTION

The surface chemistry of nanoparticles (NPs) plays a key role in controlling the interactions of nanoparticles with each other and with their surroundings.[1−11] The intentional functionalization of nanoparticles with molecular coatings such as short-chain ligands or polymeric coatings provides one approach to controlling their environmental and biological impacts.[3,5−10]

Prior studies have frequently reported that nanoparticles with cationic functional groups interact more strongly with bacterial cells compared with those functionalized with neutral or negatively charged groups,[3,5,7,9,12] These differences have frequently been attributed to the favorable electrostatic interactions between positively charged NP surfaces and negatively charged cell membranes.[2,3,10,12] NPs with cationic surfaces generally show higher cell-membrane affinity and penetration compared to anionic and neutral surfaces,[2,12−15] and NPs with a higher surface charge density lead to higher bacterial toxicity and membrane permeability.[16,17]

While the impact of cationic surface functional groups on nanoparticle−cell interactions is widely recognized as important, much less is known about how the molecular conformation of surface ligands and the resulting spatial distribution of charge affect their resulting biological impact. Prior studies have shown that differences in the arrangement of surface ligands can impact the ability of nanoparticles to

Received: March 10, 2020
Published: May 13, 2020

https://dx.doi.org/10.1021/jacs.0c02737
J. Am. Chem. Soc. 2020, 142, 10814−10823

penetrate cell membranes,[8,16−18] suggesting the importance of NP surface ligand conformation on membrane interactions. One challenge with understanding the influence of surface molecular layers is that self-assembled monolayers on gold and most other nanoparticles of interest can be easily removed or displaced under biological conditions.[19−21] Nanodiamond is an excellent platform for understand the influence of surface molecular groups because functionalization via an "all-carbon" scaffold provides outstanding stability.[22−25] In prior work using nuclear magnetic resonance (NMR) T_2 measurements, we found that when a model cationic polymer was covalently linked to diamond nanoparticles, approximately 45% of the segments are highly mobile, while the rest (∼55%) remain tightly bound on the NP surfaces.[26] In contrast, nanoparticles functionalized with short molecular linkers must have the charged groups closer to the surface.

Here, we demonstrate how the spatial distribution of charged molecular functional groups at the surface of diamond nanoparticles impacts their interactions with a Gram-negative model bacterium. Figure 1 shows the five cationic diamond NP

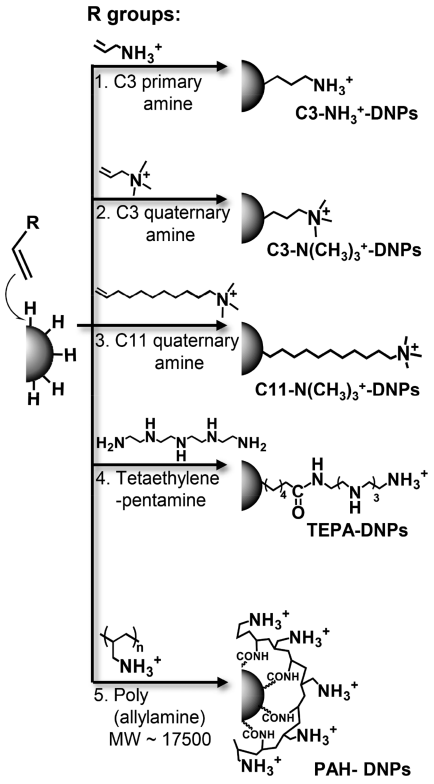

Figure 1. Functionalization scheme of five cationic amine-containing monolayer binding to 5-nm-core hydrogen-functionalized diamond nanoparticles (DNPs). Molecules and DNPs are not drawn to scale.

surfaces that we prepared using an approach we described previously.[25] To identify the influence of primary vs quaternary amino groups, we prepared diamond nanoparticles (DNPs) linked via three-carbon chains to terminal primary amino groups (C3−NH_3^+−DNPs) and quaternary (tetramethylammonium) amino groups (C3−$N(CH_3)_3^+$−DNPs. To explore the influence of chain length, we also prepared DNPs with a C11 chain terminated with a tetramethylammonium group (C11−$N(CH_3)_3^+$−DNPs). To determine the influence of charges distributed along the length of the molecules, we prepared DNPS functionalized with tetraethylenepentamine (TEPA−DNPs). Finally, to determine the influence of ligand conformational flexibility, we synthesized DNPs with a covalently bonded poly(allylamine) (PAH−DNPs). We use *Shewanella oniedensis* MR-1 (*S. oneidensis*) as a model biological organism due to its ubiquity and importance in the environment.[27,28] Previous studies have shown *S. oneidensis* to be more hardy than other Gram-negative bacteria models, signifying that any impacts measured here are likely to be amplified in other strains. In addition, working with *S. onidensis* MR-1 allows a comparison to other studies, including those with ligands similar to those studies here.[29]

Using the above surface modifications, we employed a bacterial live/dead (L/D) assay, a growth-based viability (GBV) assay, and transmission electron microscopy (TEM) to characterize how nanoparticles functionalized with these molecules interacted with *Shewanella*. Our results show that PAH−DNPs induce high cytotoxicity by disrupting the integrity of bacterial cell membranes. Surprisingly, however, the nanoparticles functionalized with shorter linear molecules all exhibited only weak association with bacterial cell membranes and little toxicity, even though their measured zeta potentials are similar to that of the PAH-modified nanoparticles. While the zeta potential is a convenient and commonly used measure of nanoparticle charge, it does not capture essential differences in molecular-level nanoparticle properties that control their biological impact. Our results suggest that the presence of conformationally flexible molecular groups extending away from the nanoparticle core and therefore able to intercalate into the outer molecular layers of bacterial cell membranes is a key molecular factor controlling the biological impact of cationic functionalized nanoparticles.

EXPERIMENTAL SECTION

Materials. All reagents were purchased from Sigma-Aldrich unless noted otherwise. Nanopure water (resistivity ≥18 MΩ·cm, Thermo Scientific Nanopure system GenPure UV-TOC/UF xCAD plus) was used for all experiments. The terminal alkenes used to functionalize diamond nanoparticles (DNPs) in this article are allyl trimethylammonium bromide, *tert*-butyl *N*-allylcarbamate (98%), 11-trimethylammonium-1-undecene bromide, and 5-hexenoic acid (98%). Allyl trimethylammonium bromide was synthesized by a reported method,[25] and 11-trimethylammonium-1-undecene bromide was synthesized by a modified procedure.[30] See the Supporting Information for detailed synthesis procedures and ^{1}H NMR and ^{13}C NMR (Supporting Information, S1). Both allyl trimethylammonium bromide and 11-trimethylammonium-1-undecene bromide absorb moisture over time to form an insoluble complex, thus they need to be stored in a moisture-free environment.

Preparation of Different Positively Charged Diamond Nanoparticle Surfaces. Detonation diamond nanoparticles (5 nm average primary particle size, Nanostructured & Amorphous Material Inc.) (DNPs) were used for the studies reported here. These DNPs were functionalized with five different positively charged ligands using a radical-based method we reported previously.[25] Figure 1 shows an overview of the functionalization process and the chemical structures of the five different positively charged DNP surfaces. The DNPs were heated in a tube furnace with a flow of pure hydrogen gas (1 atm, 50 standard cm^3 min^{-1}) at 600 °C for 6 h to hydrogen-terminate the surface atoms.[25,31] The TEM micrographs of the hydrogenated DNPs from our previous study show an average core particle size of 5 nm and no evidence for graphitic shells.[25] The reactant solution containing benzoyl peroxide (Luperox A98, > 98%), the reactant molecule of interest, and an appropriate anhydrous solvent were very briefly (∼10 min) dried over 3 Å molecular sieves to help sequester any water present in the benzoyl peroxide. The supernatant was

https://dx.doi.org/10.1021/jacs.0c02737
J. Am. Chem. Soc. 2020, 142, 10814−10823

removed, mixed with hydrogen-terminated DNPs, and held at 80 °C for 3.5 h while stirring under an argon atmosphere. The solution was cooled slowly to room temperature overnight. Details of the conditions used for functionalizing these five surfaces are included in Supporting Information (S2). The functionalized DNPs were purified by rinsing in the corresponding reaction solvent (50 mL per 50 mg of DNPs) with sonication to ensure resuspension, followed by centrifugation at 4480*g* (gravitational constant) until the samples consisted completely of pellets (typically 5−50 min). The washing and centrifugation steps were repeated with water (50 mL per 50 mg DNPs, 1×). The final samples were resuspended in 1 mM HCl solution and centrifuged at 14 400*g* for 30 min. Aggregated NPs were removed, leaving behind individual NPs and small clusters for biological studies.

Characterization of Diamond NP Surfaces. We measured the hydrodynamic diameters and zeta potentials of the functionalized DNPs using dynamic light scattering (DLS) and electrophoretic light scattering (Marvern Zetasizer ZS). The results from these measurements are provided in Supporting Information (S3). In summary, the average hydrodynamic diameter of all five types of nanoparticles after functionalization is 41.0 nm, and the average zeta potential is +42.7 mV. Chemical compositions and surface structures of all functionalized diamond nanoparticles were characterized by both X-ray photoelectron spectroscopy (XPS) and nuclear magnetic resonance (NMR). X-ray photoelectron spectroscopy (XPS) measurements were performed using a Thermo Scientific K-alpha XPS system with a microfocused monochromated Al Kα X-ray source and a 180° hemispherical analyzer with a 128-channel detector using an analyzer pass energy of 50 eV. XPS data were analyzed using Casa XPS software[32] and were energy-referenced to the C 1s peak at 284.8 eV binding energy. Samples for XPS were prepared by drop-casting 20 μL of a dilute sample onto doped silicon wafers (B-doped, 0.1−1 Ω·cm resistivity, Electrooptic Materials). NMR measurements were performed using a Bruker Avance-600 spectrometer with a TCI-F cryoprobe. To ensure quantitative results, the recycling time (d_1) was set to 10 s, which is more than 5 times longer than the T_1 of the protons of interest. Large solvent peaks were reduced in intensity using solvent suppression to achieve high-quality data. DNP samples for NMR analysis were further centrifuged down (14 100*g*) to form pellets and were redissolved in D_2O. This process replaced H_2O with D_2O as much as possible and was repeated at least three times. The samples were then further disaggregated with sonication.

Evaluation of Toxicity toward Bacteria. To evaluate the toxicity of five different cationically functionalized DNPs, we used a growth-based viability (GBV) assay.[33] *Shewanella oneidensis* MR-1 (*S. oneidensis*) was grown from a stock solution that was stored in 30% glycerol at −80 °C; the bacteria were inoculated into Luria−Bertani broth (LB) agar plates and incubated at 30 °C for 18−24 h. The resulting bacterial colonies were inoculated into 10 mL of LB broth and incubated at 30 °C for 4−6 h or until the mid-log phase. These cultures were centrifuged at 750*g* for 10 min and resuspended with 1× Dulbecco's phosphate-buffered saline (DPBS) (Corning) for 10 min. This DPBS solution was centrifuged again at 750*g* for 10 min and resuspended in HEPES buffer (2 mM, pH 7.4) to obtain a concentration with an optical density of 0.1 at 600 nm. In this study, we normalize nanoparticle doses based on the total amine concentration of the surrounding ligands, as described below. In a 96-well plate, aliquots of *Shewanella* were introduced, followed by the addition of functionalized DNPs to achieve amine concentrations (after dilution) of 1.24, 2.5, 5, 10, 20, 40, and 80 nM. After 1 h of exposure, a 5 μL aliquot was removed from each of the 96 wells and added to 195 μL of fresh LB broth in triplicate, and optical density readings were collected with a BioTek Synergy Mx Microplate Reader at 600 nm every 20 min over the course of 19 h at 30 °C and with medium intensity agitation for 1 min prior to each reading. Growth curves were analyzed as described previously.[33]

Bacterial Live/Dead Assay (L/D Assay). The LIVE/DEAD BacLight Viability Kit (ThermoFisher Scientific) was used to quantify bacterial membrane damage by different cationic DNPs. *S. oneidensis* suspensions were prepared and cultured. Functionalized DNPs were introduced into the suspensions at concentrations identical to those used in GBV measurements. Samples were then distributed in a 96-well plate in at least triplicate and were exposed to a stain consisting of a mixture of SYTO 9 dye and propidium iodide for 15 min following the manufacturer's recommendations. Briefly, fluorescence measurements were performed using a plate reader (BioTek Synergy Mx Microplate Reader) with an excitation wavelength of 485 nm and emission at 528 nm (for SYTO9 stain) and 638 nm (for propidium iodide stain). The ratio of fluorescence intensities at 528 and 638 nm, I_{528}/I_{638}, was compared with that of control samples of live and dead bacteria, yielding an average fraction of bacteria with intact membranes (live bacteria). The bacterial viability assay is based on growth rates of nanoparticle-exposed bacterial populations compared with the growth of control populations. Experimental variations between bacterial populations can yield individual measurements with calculated viability slightly greater than 100%; however, replicate measurements show that none of the measurements exceed 100% viability in a statistically significant manner.

Transmission Electron Microscopy (TEM). Transmission electron microscopy (TEM) images of *S. oneidensis* MR-1 exposed to nanodiamonds were obtained with a FEI Tecnai T12 with a 120 kV operating voltage after resin embedding. *S. oneidensis* MR-1 that was exposed to functionalized DNPs was washed in D-PBS and suspended in HEPES buffer. The exposed bacterial suspension was centrifuged down to a pellet, washed three times with 0.1 M cacodylate buffer, and fixed for 50 min in 2.5% glutaraldehyde in 0.1 M sodium cacodylate buffer. Fixed cell pellets were washed with sodium cacodylate buffer, dehydrated with increasing concentrations of ethanol solutions (30, 50, 70, 80, 90, 95, and 100% EtOH in water), and rinsed with propylene oxide three times. Then, the pellets were soaked in a 2:1 propylene oxide/epoxy resin for 2 h, a 1:1 propylene oxide/epoxy resin overnight, a fresh 1:1 propylene/epoxy resin for 5 h, and then finally fixed in pure resin in a vacuum oven. Slices of the pellet were microtomed with a Leica uC6 microtome for imaging. Sections were stained with uranyl acetate and lead citrate and placed on copper TEM grids (Ted Pella Inc.) for imaging.

Normalization of *S. oneidensis* Respons to the Amine Concentration. While biological responses to nanomaterials are frequently plotted using nanoparticle concentrations as an experimental variable, our work is aimed at understanding the effect of the charged amino functional groups. The number of amino groups per nanoparticle varies with the identity of the ligand. For example, nanoparticles functionalized with small-molecule ligands bearing a single amino group present a smaller number of amino groups compared with DNPs functionalized with cationic polymers. Therefore, to understand if this inherently higher amine content in PAH−DNPs contributes to the significantly higher membrane damage and cytotoxicity, we analyzed the responses of GBV and the L/D assay using the total concentration of exposed amine groups in each sample. We used quantitative ^{1}H NMR to determine the total concentration of amine moieties in each sample and normalized the GBV toxicity and L/D membrane damage to yield the resulting biological impact for a given concentration of amino groups. This normalization allows us to compare the bioresponses per amine among different DNP surfaces. For quantitative NMR analysis, three known amounts of each propylamine (with D_2O) [i.e., propyl trimethylamine (with D_2O), 11-trimethylamine (with D_2O), and tetraethylenepentamine (with D_2O) and poly(allylamine) (with D_2O)] were used as external standards, and peak integrations were compared to these standards. The relaxation delay was set to at least 5 times the T_1 of the standards, and integrated peak areas are normalized with the number of scans and the receiver gain.

RESULTS

Characterization of Functionalized DNPs. In order to verify that the DNPs are functionalized as expected, we characterized the functionalized DNPs using X-ray photoelectron spectroscopy (XPS). Figure 2a−e shows the N 1s spectra for all five cationic surfaces: poly(allylamine hydro-

https://dx.doi.org/10.1021/jacs.0c02737
J. Am. Chem. Soc. 2020, 142, 10814−10823

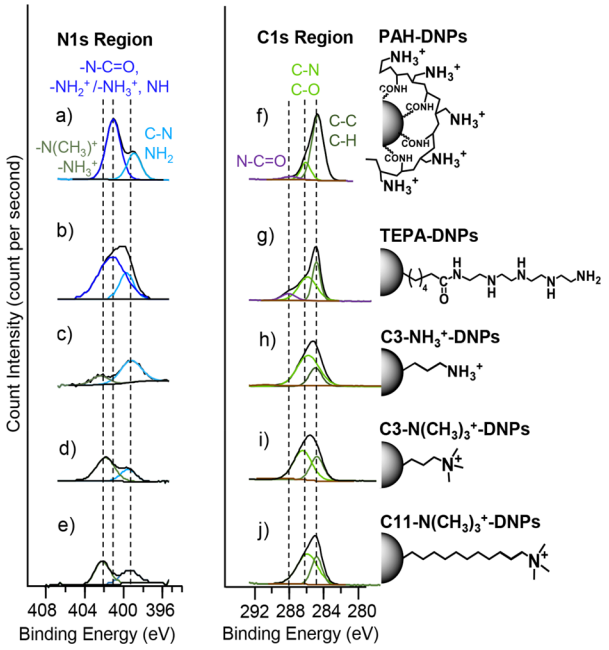

Figure 2. XPS spectra of N 1s regions (a–e) and C 1s regions (f–j) of PAH–DNPs, TEPA–DNPs, C3–NH_3^+–DNPs, C3–$N(CH_3)_3^+$–DNPs, and C11–$N(CH_3)_3^+$–DNPs.

chloride)–DNPs (PAH–DNPs, Figure 2a), tetraethylenepentamine–DNPs (TEPA–DNPs, Figure 2b), C3 primary amine–DNPs (C3–NH_3^+–DNPs, Figure 2c), C3 quaternary amine–DNPs (C3–$N(CH_3)_3^+$–DNPs, Figure 2d), and C11 quaternary amine–DNPs (C11–$N(CH_3)_3^+$–DNPs, Figure 2e). The nitrogen region for PAH–DNPs (Figure 2f) shows two peaks at 399 and 401 eV. TEPA–DNPs (Figure 2g) have two peaks at 399.6 and 401 eV. Nitrogen 1s peaks that are centered at 399–400 eV are often assigned as nonprotonated amine moieties such as C–N and $-NH_2$,[34,35] while nitrogen peaks that are at higher binding energies (400–402 eV) have been reported as amide bonds (–NH–CO) and amines that are in their protonated states ($-NH_3^+$, $-N(CH_3)_3^+$).[23,34,36] From our results shown in Figure 2a–e, the amide bond moiety at 401 eV binding energy is observed only for PAH–DNPs and TEPA–DNP and is consistent with these surface structures because the PAH and TEPA molecules are linked to the carboxylate DNP surfaces through an amide linkage. The N 1s spectra of C3–NH_3^+–DNPs (Figure 2c), C3–$N(CH_3)_3^+$–DNPs (Figure 2d), and C11–$N(CH_3)_3^+$–DNPs (Figure 2e) show two peaks that are centered at 399.6 and 402.2 eV and are consistent with the C–N nitrogen (399.6 eV)[37] and $-NH_3^+$ and $-N(CH_3)_3^+$ nitrogen (402.2 eV, protonated amines)[34,35] moieties that are present at these surfaces. Figure 2f–j shows C 1s spectra for all five cationic surfaces. The peak at 284.8 eV is present in all carbon 1s spectra and corresponds to C–C and C–H from diamond cores and hydrocarbon chains at DNP surfaces.[23] Peaks centered at 286 eV are also observed in all C 1s spectra and are consistent with the C–N moieties that are present on all of these surfaces. Nitrogen moieties such as C–N and C═N at carbon nanoparticle surfaces have been reported to appear at approximately 285.9 ± 0.1 eV.[25,35] Additional peaks at 288.1 eV are observed in PAH–DNPs (Figure 2f) and TEPA–DNPs (Figure 2g). C 1s spectra, which we attribute to C 1s atoms in amide linkages[38] (N–C═O), result from the EDC coupling. The carbon 1s spectra show consistent results with the nitrogen spectra for each cationic DNP surface, which further verified the presence of C–N, CO–NH, and $-NH_2/NH^{3+}$ moieties in our samples. XPS measurements were made and quantified independently on both Si and Au substrates (drop-cast substrates) to verify data consistency. The line shapes of N 1s and C 1s were very consistent among measurements using different drop-case substrates and among replicates (Supporting Information S4). The XPS results in Figure 2 confirm that the DNP surfaces have been functionalized with different amine moieties through covalent bonds, yielding the structures shown in Figure 1. Quantitative analysis of the XPS data (Supporting Information S5 for details) yields an average surface coverage of 0.7 ± 0.2 molecules per nm^2 for the DNPs functionalized with linear ligands, consistent with one monolayer of coverage as previously reported.[25]

Surface Structural Analysis Using NMR. While XPS analysis shows that the above procedure forms molecular layers with exposed amine groups as depicted in Figure 1, further insight into the specific chemical structures of the molecular ligands upon attachment is needed. We used ^1H NMR to characterize the functionalized NP surfaces, as shown in Figure 3 and Table 1. While a detailed analysis of the NMR data is included in the Supporting Information, several important observations are noted here. We first note that vinyl protons, which would appear in the 5 to 6 ppm region, are not observed in any of the five spectra shown in Figure 3. This result demonstrates that the terminal vinyl groups of the starting ligands have reacted in the course of the above procedure and that the ligands are attached to the DNP surface through the vinyl terminus. Further confirmation of the chemical structure of the surface-attached molecules is obtained from a more detailed analysis of the spectra (Supporting Information S6). Table 1 summarizes the assignments and chemical species types for all peaks in the ^1H NMR spectra of the five amine-functionalized DNP surfaces. The ^1H NMR data in Figure 3 provide detailed structure confirmation that the five cationic surfaces have the chemical structures depicted in Figure 1. As described in the Experimental Section, in order to help understand the roles of amino groups in controlling the biological impact and toxicity of cationic nanoparticles, we quantify the total concentration of amino groups for each DNP surface by integrating the areas of peaks that are characteristic of amine moieties (labeled as c, f, g, i, j, l_{1-8}, m, n, and o). The measured concentrations of amino groups in the stock samples are included in Supporting Information S6, Table S3. All functionalized DNP solutions were then diluted to the same amino group concentration for bacterial exposure.

Biological Impact of Cationic DNPs on *S. oneidensis*. Growth-Based Viability and Live/Dead Assay. We examined the influence of the five different positively charged amine-functionalized DNPs on Gram-negative bacterium *Shewanella oneidensis* MR-1 (*S. oneidensis*) using a growth-based viability assay.[33] Figure 4a shows the viability of *S. oneidensis* after the introduction of functionalized DNPs for 1 h, reported for different concentrations of surface-tethered amino groups. None of the DNPs functionalized with small-molecule ligands (e.g., C3–$N(CH_3)_3^+$–DNPs, C3–NH_3^+–DNPs, C11–$N(CH_3)_3^+$–DNPs, and TEPA–DNPs) have a significant negative influence on the viability of *S. oneidensis* over the concentration range studied. In contrast, the PAH–DNPs show significant toxicity even at a low amine concentration of 10 nM (equivalent DNP concentration: 0.4

https://dx.doi.org/10.1021/jacs.0c02737
J. Am. Chem. Soc. 2020, 142, 10814–10823

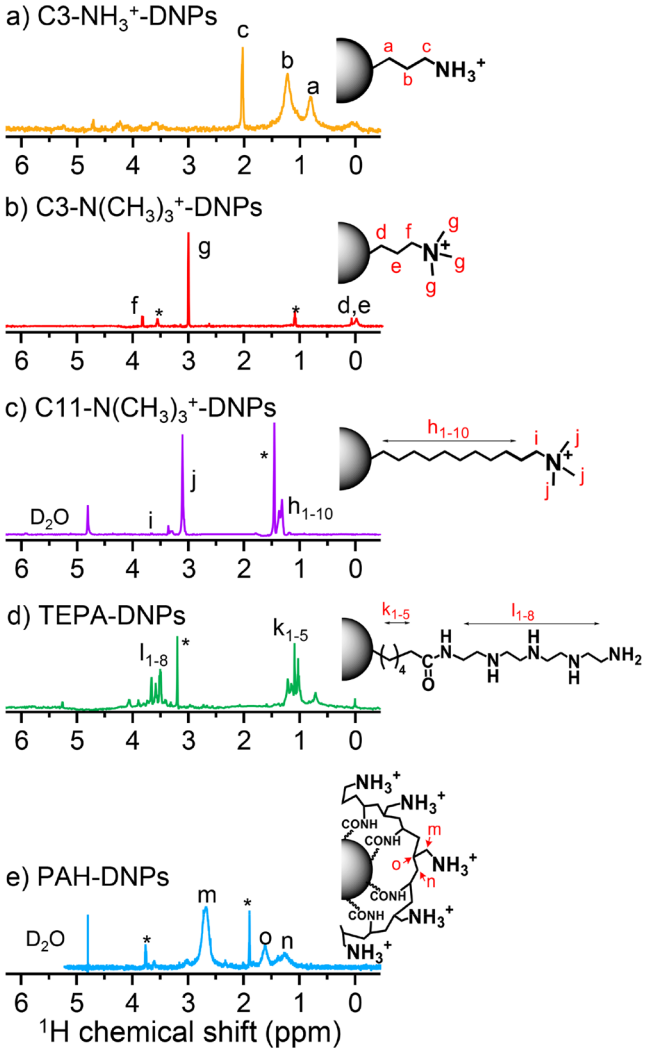

Figure 3. ^{1}H NMR spectra of a) C3−NH_3^+−DNPs, b) C3−$N(CH_3)_3^+$−DNPs c) C11−$N(CH_3)_3^+$−DNPs, d) TEPA−DNPs and e) PAH−DNPs. Asterisk denotes for solvent peaks.

Table 1. Peak Assignment for ^{1}H NMR Spectra of Amine-Functionalized DNP Surfaces

DNP surfaces	^{1}H δ(ppm)	assignment	type
C3−NH_3^+	0.8	a	$-(CH_2)_n$
	1.2	b	$-(CH_2)_n$
	2.03	c	$-CH_2NH_3^+$
C3−$N(CH_3)_3^+$	0.07−0.15	d, e	$-(CH_2)_n$
	3.1	g	$-N(CH_3)_3^+$
	3.9	f	$-CH_2N(CH_3)_3^+$
C11−$N(CH_3)_3^+$	1.33	h_{1-10}	$-(CH_2)_n$
	3.11	j	$-N(CH_3)_3^+$
	3.35	i	$-CH_2N(CH_3)_3^+$
TEPA	1.02−1.21	k_{1-5}	$-(CH_2)_n$
	3.46−3.66	l_{1-8}	$-CH_2NH$
			$-CH_2NH_2$
PAH	1.17	n	$-CH_2$
	1.59	o	$-CH-CH_2$
	2.67	m	$-CH_2NH_3^+$

mg/L) and induce 100% cell death at 20 nM amine concentration (DNPs: 0.8 mg/L) and above. To confirm that the toxicity is a nanoparticle surface-specific effect, we also conducted control studies exposing *S. oneidensis* to the free ligands. As shown in Figure 4b, none of the ligands, including PAH, show any toxicity across the same amine concentration range. Thus, we conclude that the toxicity of PAH is observed only when it is attached to the DNPs and is therefore a nanoparticle-surface-specific effect. To understand the specific interactions that led to the high cytotoxicity, we employed the live/dead (L/D) assay to quantify the membrane integrity of the cells.[39−41] The L/D assay is a fluorescence-based method that uses two different fluorescent dyes that bind to nucleic acid: green fluorescent SYTO 9 and red fluorescent propidum iodide (PI) dyes.[42] These two stains have different abilities to penetrate healthy bacterial cells: the SYTO9 stain (excitation at 485 nm, emission at 528 nm) is membrane-permeant, whereas the PI stain (excitation at 485 nm, emission at 638 nm) only crosses damaged cell membranes. Figure 4c shows the influence of the five cationic DNPs on the integrity of cell membranes of *S. oneidensis*, presented as ratios of the fluorescence intensity of SYTO9 to the PI stain that were exposed with NP-cell matrixes. Because the signals from the SYTO9 stain represent all cells and signals from the PI stain represent only cells with damaged membranes, the fluorescence intensity ratio of SYTO9 to PI is related to the fraction of cells with intact membranes. The L/D assay exhibits the same trend as the GBV assay where the four DNPs functionalized with small-molecule ligands (C3−$N(CH_3)_3^+$−DNPs, C3−NH_3^+−DNPs, C11−$N(CH_3)_3^+$−DNPs, and TEPA−DNPs) had almost no effect on the integrity of the *S. oneidensis* membrane, while PAH−DNPs induce significant membrane damage (20% of all cells having damaged membranes) at 10 nM amine concentration (DNPs: 0.4 mg/L) and up to 60% membrane damage at higher amine concentration (Figure 4c).

The results from the L/D control studies using free ligands (Figure 4d) are consistent with the results of GBV measurements, showing that none of the free ligands (including PAH) induce significant membrane damage across the same concentration range, while the covalently linked PAH polymer induces membrane damage when attached to the DNP surface. The reduced viability revealed by the GBV assay and the membrane damage revealed by the L/D assays demonstrate that amino groups present in an amino-containing polymer (such as PAH) induce very strong biological interactions compared with the same concentration of primary or quaternary amino groups that are tethered more closely to the DNP surfaces (such as linear ligands with terminal amino groups). We further note that if we had instead presented these data as a function of nanoparticle concentration instead of amino concentration, then the strong interactions of PAH would be even more apparent because of the higher ligand density of PAH-NDPs per nanoparticle (Supporting Information S7). Prior studies have often correlated the toxicity of nanoparticles with the presence of a net positive charge.[2,13−15] However, recent studies using both experiments and MD simulations have suggested that, at high amine densities, both the total number of charged groups and the fraction of amine in a charged state can be less than those at intermediate coverages due to Coulombic interactions between neighboring sites.[43,44] We measured the zeta potential (ζ potential) for all five cationic surfaces in both nanopure water and HEPES buffer because this is the biological exposure medium. Figure 4e shows that the ζ potentials for the DNPs that are functionalized with linear small-molecule ligands (C3−NH_3^+−

https://dx.doi.org/10.1021/jacs.0c02737
J. Am. Chem. Soc. 2020, 142, 10814−10823

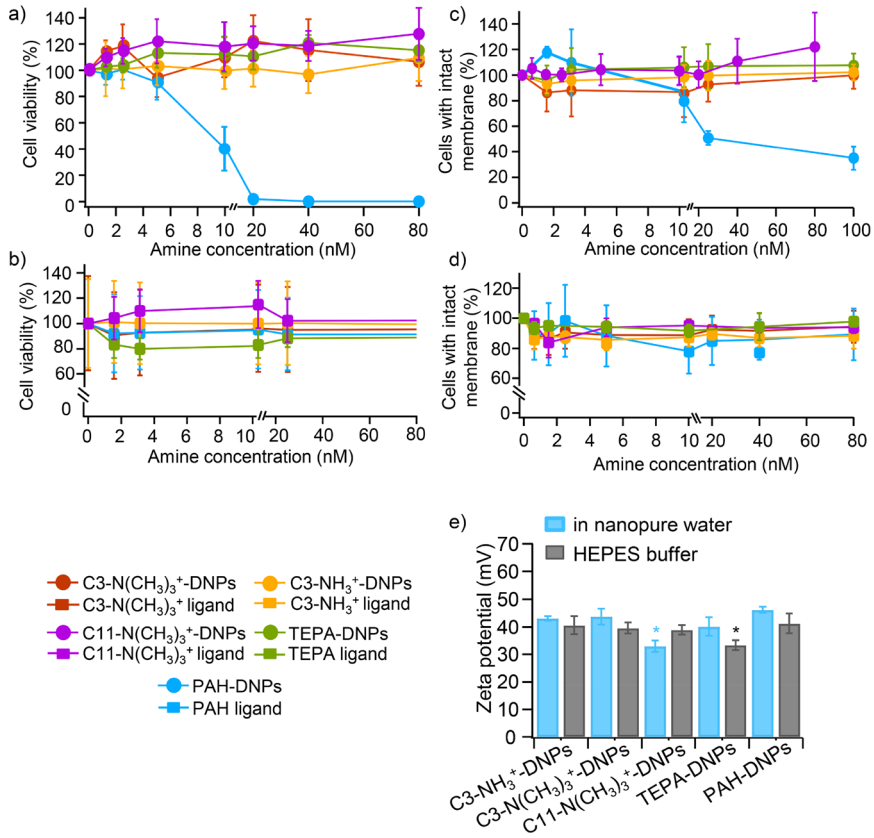

Figure 4. Growth-based viability results of *S. oneidensis* upon exposure to all cationic diamond nanoparticles (a) and free cationic ligands (b) (n = 4), with the bacterial live/dead assay results assessing the membrane integrity of *S. oneidensis* by all cationic DNPs (c) and free cationic ligands (d) (n = 6). (e) ζ-potential values of all cationic DNPs in HEPES buffer (bacterial medium) (n > 5 from technical replicates). The asterisk denotes statistical differences among measurements using one-way ANOVA Tukey's multiple comparison test (p < 0.05). All error bars represent the standard deviation.

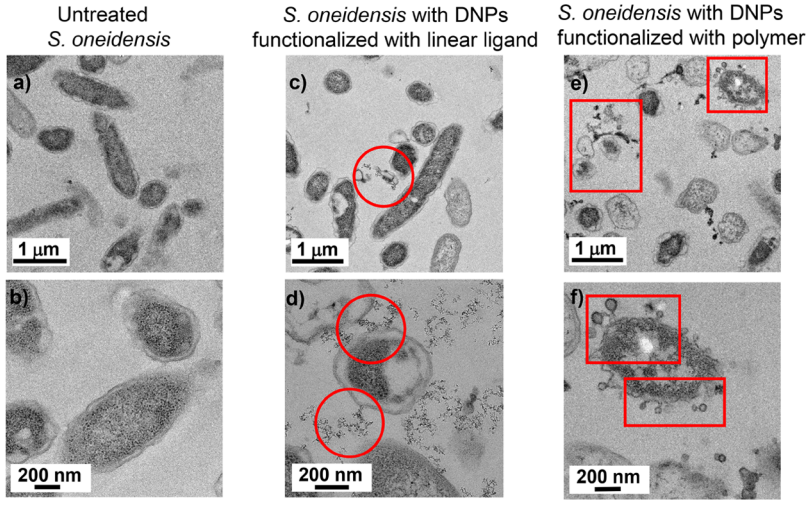

Figure 5. TEM images of (a, b) healthy *S. oneidensis* without exposure to cationic DNPs, (c, d) *S. oneidensis* after exposure to linear-molecular-ligand-functionalized DNPs (C3−N$(CH_3)_3^+$−DNPs), and (e, f) *S. oneidensis* after exposure to polymer-functionalized DNPs (PAH−DNPs). TEM images were taken using *S. oneidensis* that was treated with 80 nM amine at DNP surfaces.

DNPs, C3−N$(CH_3)_3^+$−DNPs, C11−N$(CH_3)_3^+$−DNPs, and TEPA−DNPs) and the DNPs that are functionalized with polymer (PAH−DNPs) are statistically identical, except for TEPA−DNPs with slightly lower ζ potentials. The previous molecular dynamics studies have shown that when the net surface charge density is sufficiently high, the zeta potential is only weakly dependent on the density of surface charges due to charge compensation by the counterions.[45−47] In the present work, charge compensation by counterions likely plays a role in controlling the zeta potential such that the multicationic PAH shows a zeta potential that is almost identical to that of the monocationic molecular ligand at DNP surfaces. An important conclusion from this work is that the ζ potential alone is not a good parameter for predicting the biological impact of

https://dx.doi.org/10.1021/jacs.0c02737
J. Am. Chem. Soc. 2020, 142, 10814−10823

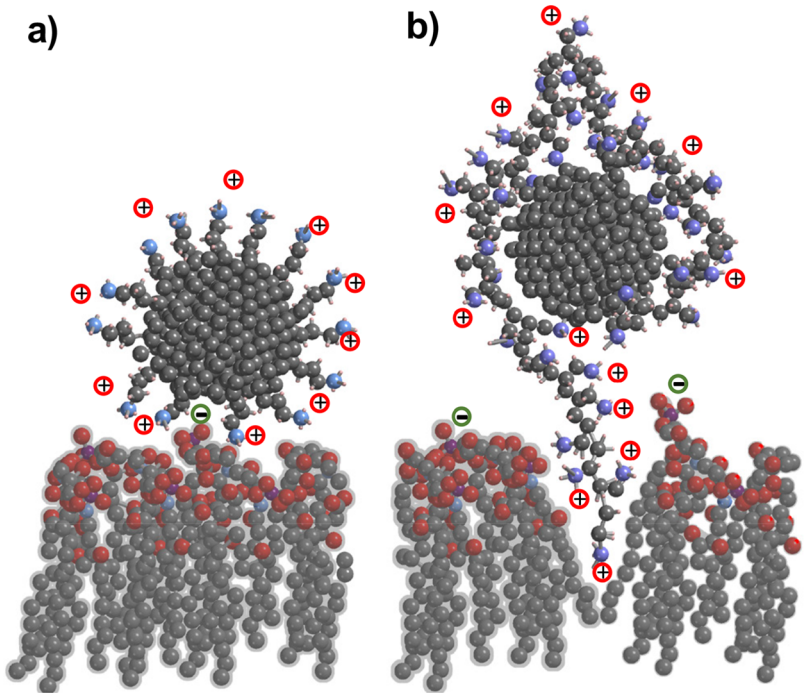

Figure 6. Conceptual illustration depicting the spatial distribution of charge of DNPs functionalized with (a) linear molecular ligands and (b) covalently linked polymer interacting with a model LPS layer. While short molecular ligands interact only with the outermost regions of the LPS layers of the cellular membrane, loops and tails of the polymer can insert into the layers, leading to membrane disruption. Gray spheres represent C atoms; red, O atoms; blue, N atoms; and purple, P atoms of LPS. Positive charges correspond to amino groups; negative charges correspond to phosphate groups of LPS.

functionalized nanoparticles. Overall, the GBV toxicity and L/D assay results show that the DNPs functionalized with the small linear molecules do not have any negative effect on the *S. oneidensis* viability or on the membrane integrity while the PAH-functionalized DNPs induce significant cell death and membrane damage even at lower concentrations. These results show that neither the amine concentration nor the surface charge (measured by the ζ potential) is the key factor in this difference; rather, the ligand conformation and spatial distribution of amino groups must be playing important roles in controlling the biological interactions.

Cell Membrane Deformation Induced by Polyamine-Functionalized DNPs. To determine the influence of functionalized DNPs on *S. oneidensis* cell membranes, we analyzed the structure of *S. oneidensis* cell membranes after exposure to functionalized DNPs using TEM. Since all four small-molecule ligand-functionalized DNPs show similar responses in GBV and the L/D assay, we chose C3−$N(CH_3)_3^+$−DNPs as a representative linear ligand for comparison with PAH−DNPs. Figure 5a,b shows TEM images of untreated *S. oneidensis* cells in bright-field imaging mode. Figure 5c,d shows two representative TEM images of the bacterial cells after exposure to C3−$N(CH_3)_3^+$−DNPs; no major membrane distortion or disruption is visible, and the DNPs appear to be adhered to the outer layer of the cell membranes (indicated by the red circle). In contrast, Figure 5e,f shows TEM images of the bacterial cells after exposure to PAH−DNPs. In this case, we observe significant membrane distortion with spherical protrusions on the outside of the bacterial membranes (indicated by red squares). These structures appear to be similar to previously reported images of outer membrane vesicles (OMVs).[48−50] Prior work has shown that OMVs can be formed as a stress response.[51] Similarly, the structures observed in our studies may be an indication of stress induced by PAH−DNPs. We have included a larger TEM image in Supporting Information S8. In summary, the TEM images in Figure 5 demonstrate that the *S. oneidensis* cell surfaces respond much more strongly to the NPs functionalized with the polymer PAH compared with NPs functionalized with the linear small-molecule ligand, even when the total concentration of amine groups is the same.

Role of Molecular Structure. Although the strong correlation between bacteria viability (Figure 4a,b) and membrane damage (Figure 4c,d and 5) was expected, our overall results are surprising in two ways. First, control experiments using the free PAH cationic polymer show that the free PAH polymer does not induce membrane damage or a decrease in cell viability across the tested amine concentrations. The cytotoxicity of PAH−DNPs results only from surface-attached PAH polymers. Second, both GBV and L/D assays show that on a per amine basis, each amino group of PAH−DNPs induces significantly higher toxicity than an equal number of amino groups on a linear small-molecule ligand. Viability measurements normalized to the amino concentration (Figure 4a−d) show that the concentration of surface-exposed amino groups in solution is not the key factor in this difference nor is the zeta potential. Dielectrophoretic light scattering estimates the zeta potential by measuring the dielectrophoretic mobility and within using a model (such as the widely used Smoluchowski model[48,51−53] to relate the measured mobility to a zeta potential. However, this approach assumes that particles are hard spheres with a uniform charge distribution and does not account for lateral inhomogeneities across the NP surfaces or a more extended distribution of charge in the electric double layer.[54,55] Consequently, measurements of the zeta potentials of DNPs functionalized with molecules having

https://dx.doi.org/10.1021/jacs.0c02737
J. Am. Chem. Soc. 2020, 142, 10814−10823

different morphologies (e.g., linear ligands vs polymer-linked) do not adequately represent the differences in the spatial distribution of charge. Our results show that the spatial distribution of charge plays a key role in nanoparticle−membrane interactions. The main difference between DNPs functionalized with linear ligands (such as C3−NH_3^+−DNPs) and those modified with covalent-bonded polymers (PAH−DNPs) is the conformation of the surface molecules. Figure 6 represents a schematic illustration of functionalized DNPs interacting with a model LPS layer. For DNPs that are functionalized with short linear molecules, the charges are located in a thin shell at the periphery of the molecular monolayer, as shown in Figure 6a. In contrast, DNPs that are functionalized with polymers have charges that extend further from the nanoparticle surface. In prior work, we characterized the molecular conformations of DNPs covalently bonded to PAH.[26] Our NMR T_2 measurements showed that the PAH molecules exhibited two distinct populations, corresponding to sites bonded to the surface and other sites consisting of highly flexible polymer loops and tails. Similar conformations have been reported for other polymers at planar and nanoparticle surfaces.[56−60] The presence of loops and tails leads to an average charge distributed over a finite thickness adjacent to the DNP surfaces, extending the double-layer and increasing the hydrodynamic thickness. These effects are reflected in the larger hydrodynamic diameter (d_h = 61.6 ± 2.2 nm) of DNPs modified with PAH compared with DNPs modified with linear ligands (d_h ≈ 30 nm). Other prior studies of polymer-modified nanoparticles have reported similar morphologies,[26,59,61] with loops and exposed tails extending into the adjacent liquid medium.[56,58,60] We propose that these loops and tails are largely responsible for the interaction of the PAH−NPs with *S. oneidensis* cell membranes. Specifically, we attribute the differential toxicity of PAH−ND and linear small-molecule-functionalized DNPs to differences in the radial extent of the charged groups. Prior work[29] using molecular dynamics simulations has demonstrated that PAH binds to the LPS layer in Gram-negative bacteria through electrostatic interactions and eventually migrates to the core region of the LPS. Therefore, we propose that it is the larger radial extent of the loops and tails of the surface-linked PAH polymer that enables penetration of the PAH (and its associated amino groups) into the lipopolysaccharide (LPS) layer at the surface of the Gram-negative *S. oneidensis* cell membrane. The positive charges allow the cationic NPs to bind to the surface of the bacterial membrane through electrostatic interactions, and the conformationally flexible PAH loops and tails assist physical insertion into the LPS layer.

CONCLUSIONS

These studies demonstrate that while cationic charged groups can enhance the nanoparticle interaction with cellular membranes, the detailed molecular structure of the molecules, which controls the spatial distribution and presentation of charged groups, plays a key role. While nanoparticle charges are frequently characterized using the zeta potential, this single parameter does not fully capture the essential molecular aspects that control the nanoparticle interactions. Our work indicates that the biological impact of cationic nanoparticles is greatest when the molecular functional groups extend away from the nanoparticle core in a flexible manner that can facilitate penetration of the molecules into the outermost molecular layers of the bacterial membrane. This work provides new perspectives on why cationic surface layers induce membrane damage in bacterial cells and will facilitate a further understanding of the fundamental mechanisms of cell membrane interactions of engineered NPs.

ASSOCIATED CONTENT

Supporting Information

The Supporting Information is available free of charge at https://pubs.acs.org/doi/10.1021/jacs.0c02737.

Procedures of 11-trimethylamine-1-undecene bromide synthesis and characterization, details of DNP functionalization conditions, hydrodynamic size and zeta potential analysis of functionalized DNPs, XPS quantification of functionalized-DNPs, biological responses plot of *S. oneidensis* versus NP concentration, and additional TEM images of NP-exposed *S. oneidensis* (PDF)

AUTHOR INFORMATION

Corresponding Author

Robert J. Hamers − *University of Wisconsin—Madison, Department of Chemistry, Madison, Wisconsin 53706, United States;* orcid.org/0000-0003-3821-9625; Email: rjhamers@wisc.edu

Authors

Yongqian Zhang − *University of Wisconsin—Madison, Department of Chemistry, Madison, Wisconsin 53706, United States;* orcid.org/0000-0001-9637-5314

Natalie V. Hudson-Smith − *University of Minnesota Twin Cities, Department of Chemistry, Minneapolis, Minnesota 55455, United States;* orcid.org/0000-0002-2642-0711

Seth D. Frand − *Augsburg University, Department of Chemistry, Minneapolis, Minnesota 55454, United States*

Meghan S. Cahill − *University of Minnesota Twin Cities, Department of Chemistry, Minneapolis, Minnesota 55455, United States;* orcid.org/0000-0002-1514-7625

Larissa S. Davis − *University of Wisconsin—Madison, Department of Chemistry, Madison, Wisconsin 53706, United States*

Z. Vivian Feng − *Augsburg University, Department of Chemistry, Minneapolis, Minnesota 55454, United States;* orcid.org/0000-0002-3329-3781

Christy L. Haynes − *University of Minnesota Twin Cities, Department of Chemistry, Minneapolis, Minnesota 55455, United States;* orcid.org/0000-0002-5420-5867

Complete contact information is available at: https://pubs.acs.org/10.1021/jacs.0c02737

Funding

National Science Foundation (CHE-1503408), National Science Foundation (00039202), National Science Foundation (DMR-1720415), and National Institutes of Health (S10OD012245).

Notes

The authors declare no competing financial interest.

ACKNOWLEDGMENTS

This work was supported by the National Science Foundation under the Center for Sustainable Nanotechnology (CHE-1503408). The CSN is part of the Centers for Chemical Innovation Program. N.V.H.-S. acknowledges support through

the National Science Foundation Graduate Research Fellowship Program (00039202). XPS studies used facilities and instrumentation supported by NSF through the University of Wisconsin Materials Research Science and Engineering Center (DMR-1720415). The Bruker Avance 600 NMR instrument used in this work was supported by the National Institutes of Health grant S10OD012245. Parts of this work were carried out in the Characterization Facility, University of Minnesota, which receives partial support from the NSF through the MRSEC program.

■ ABBREVIATIONS

DNPs, diamond nanoparticles; XPS, X-ray photoelectron spectroscopy; NMR, nuclear magnetic resonance; PAH, poly(allylamine hydrochloride)

■ REFERENCES

(1) Klaine, S. J.; Alvarez, P. J. J.; Batley, G. E.; Fernandes, T. F.; Handy, R. D.; Lyon, D. Y.; Mahendra, S.; McLaughlin, M. J.; Lead, J. R. Nanomaterials in the environment: Behavior, fate, bioavailability, and effects. *Environ. Toxicol. Chem.* **2008**, *27*, 1825−1851.
(2) Verma, A.; Stellacci, F. Effect of surface properties on nanoparticle−cell interactions. *Small* **2010**, *6*, 12−21.
(3) Fleischer, C. C.; Payne, C. K. Nanoparticle Surface Charge Mediates the Cellular Receptors Used by Protein-Nanoparticle Complexes. *J. Phys. Chem. B* **2012**, *116*, 8901−8907.
(4) Albanese, A.; Tang, P. S.; Chan, W. C. W. The effect of nanoparticle size, shape, and surface chemistry on biological systems. *Annu. Rev. Biomed. Eng.* **2012**, *14*, 1−16.
(5) Cho, E. C.; Xie, J. W.; Wurm, P. A.; Xia, Y. N. Understanding the role of surface charges in cellular adsorption versus internalization by selectively removing gold nanoparticles on the cell surface with a I_2/KI etchant. *Nano Lett.* **2009**, *9*, 1080−1084.
(6) Setyawati, M. I.; Mochalin, V. N.; Leong, D. T. Tuning endothelial permeability with functionalized nanodiamonds. *ACS Nano* **2016**, *10*, 1170−1181.
(7) Silva, T.; Pokhrel, L. R.; Dubey, B.; Tolaymat, T. M.; Maier, K. J.; Liu, X. F. Particle size, surface charge and concentration dependent ecotoxicity of three organo-coated silver nanoparticles: Comparison between general linear model-predicted and observed toxicity. *Sci. Total Environ.* **2014**, *468*, 968−976.
(8) Verma, A.; Uzun, O.; Hu, Y.; Hu, Y.; Han, H.-S.; Watson, N.; Chen, S.; Irvine, D. J.; Stellacci, F. Surface-structure-regulated cell-membrane penetration by monolayer-protected nanoparticles. *Nat. Mater.* **2008**, *7*, 588−595.
(9) Verma, A.; Arshad, F.; Ahmad, K.; Goswami, U.; Samanta, S. K.; Sahoo, A. K.; Sk, M. P. Role of surface charge in enhancing antibacterial activity of fluorescent carbon dots. *Nanotechnology* **2020**, *31*, 095101.
(10) Huang, K.; Hu, Y.; Yu, C. J.; Boerhan, R.; Jiang, G. Q. Charged surface groups of nanoparticles and the adsorbed proteins codetermine the fate of nanoparticles upon interacting with cells. *RSC Adv.* **2016**, *6*, 58315−58324.
(11) Mensch, A. C.; Hernandez, R. T.; Kuether, J. E.; Torelli, M. D.; Feng, Z. V.; Hamers, R. J.; Pedersen, J. A. Natural organic matter concentration impacts the interaction of functionalized diamond nanoparticles with model and actual bacterial membranes. *Environ. Sci. Technol.* **2017**, *51*, 11075−11084.
(12) Feng, Z. V.; Gunsolus, I. L.; Qiu, T. A.; Hurley, K. R.; Nyberg, L. H.; Frew, H.; Johnson, K. P.; Vartanian, A. M.; Jacob, L. M.; Lohse, S. E. Impacts of gold nanoparticle charge and ligand type on surface binding and toxicity to Gram-negative and Gram-positive bacteria. *Chem. Sci.* **2015**, *6*, 5186−5196.
(13) Goodman, C. M.; McCusker, C. D.; Yilmaz, T.; Rotello, V. M. Toxicity of gold nanoparticles functionalized with cationic and anionic side chains. *Bioconjugate Chem.* **2004**, *15*, 897−900.
(14) Arvizo, R. R.; Miranda, O. R.; Thompson, M. A.; Pabelick, C. M.; Bhattacharya, R.; Robertson, J. D.; Rotello, V. M.; Prakash, Y.; Mukherjee, P. Effect of nanoparticle surface charge at the plasma membrane and beyond. *Nano Lett.* **2010**, *10*, 2543−2548.
(15) Fleischer, C. C.; Payne, C. K. Nanoparticle−cell interactions: molecular structure of the protein corona and cellular outcomes. *Acc. Chem. Res.* **2014**, *47*, 2651−2659.
(16) Hong, S.; Leroueil, P. R.; Janus, E. K.; Peters, J. L.; Kober, M.-M.; Islam, M. T.; Orr, B. G.; Baker, J. R., Jr; Banaszak Holl, M. M. Interaction of polycationic polymers with supported lipid bilayers and cells: nanoscale hole formation and enhanced membrane permeability. *Bioconjugate Chem.* **2006**, *17*, 728−734.
(17) Giljohann, D. A.; Seferos, D. S.; Patel, P. C.; Millstone, J. E.; Rosi, N. L.; Mirkin, C. A. Oligonucleotide loading determines cellular uptake of DNA-modified gold nanoparticles. *Nano Lett.* **2007**, *7*, 3818−3821.
(18) Herbig, M. E.; Assi, F.; Textor, M.; Merkle, H. P. The cell penetrating peptides pVEC and W2-pVEC induce transformation of gel phase domains in phospholipid bilayers without affecting their integrity. *Biochemistry* **2006**, *45*, 3598−3609.
(19) Perera, G. S.; Athukorale, S. A.; Perez, F.; Pittman, C. U.; Zhang, D. Facile displacement of citrate residues from gold nanoparticle surfaces. *J. Colloid Interface Sci.* **2018**, *511*, 335−343.
(20) Stobiecka, M.; Deeb, J.; Hepel, M. Ligand exchange effects in gold nanoparticle assembly induced by oxidative stress biomarkers: Homocysteine and cysteine. *Biophys. Chem.* **2010**, *146*, 98−107.
(21) Ackerson, C. J.; Sykes, M. T.; Kornberg, R. D. Defined DNA/nanoparticle conjugates. *Proc. Natl. Acad. Sci. U. S. A.* **2005**, *102*, 13383−13385.
(22) Yang, W.; Auciello, O.; Butler, J. E.; Cai, W.; Carlisle, J. A.; Gerbi, J. E.; Gruen, D. M.; Knickerbocker, T.; Lasseter, T. L.; Russell, J. N.; Smith, L. M.; Hamers, R. J. DNA-modified nanocrystalline diamond thin-films as stable, biologically active substrates. *Nat. Mater.* **2002**, *1*, 253−257.
(23) Stavis, C.; Clare, T. L.; Butler, J. E.; Radadia, A. D.; Carr, R.; Zeng, H.; King, W. P.; Carlisle, J. A.; Aksimentiev, A.; Bashir, R.; Hamers, R. J. Surface functionalization of thin-film diamond for highly stable and selective biological interfaces. *Proc. Natl. Acad. Sci. U. S. A.* **2011**, *108*, 983−988.
(24) Krueger, A.; Lang, D. Functionality is key: recent progress in the surface modification of nanodiamond. *Adv. Funct. Mater.* **2012**, *22*, 890−906.
(25) Zhang, Y.; Abbaspour Tamijani, A.; Taylor, M. E.; Zhi, B.; Haynes, C. L.; Mason, S. E.; Hamers, R. J. Molecular surface functionalization of carbon materials via radical-induced grafting of terminal alkenes. *J. Am. Chem. Soc.* **2019**, *141*, 8277−8288.
(26) Zhang, Y.; Fry, C. G.; Pedersen, J. A.; Hamers, R. J. Dynamics and morphology of nanoparticle-linked polymers elucidated by nuclear magnetic resonance. *Anal. Chem.* **2017**, *89*, 12399−12407.
(27) Hau, H. H.; Gralnick, J. A. Ecology and biotechnology of the genus. *Annu. Rev. Microbiol.* **2007**, *61*, 237−258.
(28) Qiu, T.; Bozich, J.; Lohse, S.; Vartanian, A.; Jacob, L.; Meyer, B.; Gunsolus, I.; Niemuth, N.; Murphy, C.; Haynes, C. Gene expression as an indicator of the molecular response and toxicity in the bacterium *Shewanella oneidensis* and the water flea *Daphnia magna* exposed to functionalized gold nanoparticles. *Environ. Sci.: Nano* **2015**, *2*, 615−629.
(29) Buchman, J. T.; Rahnamoun, A.; Landy, K. M.; Zhang, X.; Vartanian, A. M.; Jacob, L. M.; Murphy, C. J.; Hernandez, R.; Haynes, C. L. Using an environmentally-relevant panel of Gram-negative bacteria to assess the toxicity of polyallylamine hydrochloride-wrapped gold nanoparticles. *Environ. Sci.: Nano* **2018**, *5*, 279−288.
(30) Vigderman, L.; Manna, P.; Zubarev, E. R. Quantitative replacement of cetyl trimethylammonium bromide by cationic thiol ligands on the surface of gold nanorods and their extremely large uptake by cancer cells. *Angew. Chem., Int. Ed.* **2012**, *51*, 636−641.
(31) Williams, O. A.; Hees, J.; Dieker, C.; Jäger, W.; Kirste, L.; Nebel, C. E. Size-dependent reactivity of diamond nanoparticles. *ACS Nano* **2010**, *4*, 4824−4830.

https://dx.doi.org/10.1021/jacs.0c02737
J. Am. Chem. Soc. 2020, 142, 10814−10823

(32) Fairley, N. *CasaXPS*, version 2.3. 14; Casa Software Ltd, 1999; Vol. *2005*.
(33) Qiu, T. A.; Nguyen, T. H. T.; Hudson-Smith, N. V.; Clement, P. L.; Forester, D.-C.; Frew, H.; Hang, M. N.; Murphy, C. J.; Hamers, R. J.; Feng, Z. V. Growth-based bacterial viability assay for interference-free and high-throughput toxicity screening of nanomaterials. *Anal. Chem.* **2017**, *89*, 2057−2064.
(34) Strother, T.; Hamers, R. J.; Smith, L. M. Covalent attachment of oligodeoxyribonucleotides to amine-modified Si (001) surfaces. *Nucleic Acids Res.* **2000**, *28*, 3535−3541.
(35) Ederer, J.; Janoš, P.; Ecorchard, P.; Tolasz, J.; Štengl, V.; Beneš, H.; Perchacz, M.; Pop-Georgievski, O. Determination of amino groups on functionalized graphene oxide for polyurethane nanomaterials: XPS quantitation vs. functional speciation. *RSC Adv.* **2017**, *7*, 12464−12473.
(36) Baker, S. E.; Cai, W.; Lasseter, T. L.; Weidkamp, K. P.; Hamers, R. J. Covalently bonded adducts of deoxyribonucleic acid (DNA) oligonucleotides with single-wall carbon nanotubes: synthesis and hybridization. *Nano Lett.* **2002**, *2*, 1413−1417.
(37) Bogdanowicz, R.; Sawczak, M.; Niedzialkowski, P.; Zieba, P.; Finke, B.; Ryl, J.; Karczewski, J.; Ossowski, T. Novel functionalization of boron-doped diamond by microwave pulsed-plasma polymerized allylamine film. *J. Phys. Chem. C* **2014**, *118*, 8014−8025.
(38) Wang, X.; Ruther, R. E.; Streifer, J. A.; Hamers, R. J. UV-induced grafting of alkenes to silicon surfaces: photoemission versus excitons. *J. Am. Chem. Soc.* **2010**, *132*, 4048−4049.
(39) Miller, J. S.; Quarles, J. M. Flow cytometric identification of microorganisms by dual staining with FITC and PI. *Cytometry* **1990**, *11*, 667−675.
(40) Lloyd, D.; Hayes, A. J. Vigour, vitality and viability of microorganisms. *FEMS Microbiol. Lett.* **1995**, *133*, 1−7.
(41) Bunthof, C. J.; van Schalkwijk, S.; Meijer, W.; Abee, T.; Hugenholtz, J. Fluorescent method for monitoring cheese starter permeabilization and lysis. *Appl. Environ. Microbiol.* **2001**, *67*, 4264−4271.
(42) Mah, T.-F.; Pitts, B.; Pellock, B.; Walker, G. C.; Stewart, P. S.; O'Toole, G. A. A genetic basis for *Pseudomonas aeruginosa* biofilm antibiotic resistance. *Nature* **2003**, *426*, 306−310.
(43) Zheng, Z.; Saar, J.; Zhi, B.; Qiu, T. A.; Gallagher, M. J.; Fairbrother, D. H.; Haynes, C. L.; Lienkamp, K.; Rosenzweig, Z. Structure−Property Relationships of Amine-rich and Membrane-Disruptive Poly (oxonorbornene)-Coated Gold Nanoparticles. *Langmuir* **2018**, *34*, 4614−4625.
(44) Hong, J.; Hamers, R. J.; Pedersen, J. A.; Cui, Q. A hybrid molecular dynamics/multiconformer continuum electrostatics (MD/MCCE) approach for the determination of surface charge of nanomaterials. *J. Phys. Chem. C* **2017**, *121*, 3584−3596.
(45) Manning, G. S. Counterion Condensation on Charged Spheres, Cylinders, and Planes. *J. Phys. Chem. B* **2007**, *111*, 8554−8559.
(46) Manning, G. S. The Interaction between a Charged Wall and Its Counterions: A Condensation Theory. *J. Phys. Chem. B* **2010**, *114*, 5435−5440.
(47) Dreier, L. B.; Nagata, Y.; Lutz, H.; Gonella, G.; Hunger, J.; Backus, E. H. G.; Bonn, M. Saturation of charge-induced water alignment at model membrane surfaces. *Science Advances* **2018**, *4*, eaap7415.
(48) Subramanian, P.; Pirbadian, S.; El-Naggar, M. Y.; Jensen, G. J. Ultrastructure of *Shewanella oneidensis* MR-1 nanowires revealed by electron cryotomography. *Proc. Natl. Acad. Sci. U. S. A.* **2018**, *115*, E3246−E3255.
(49) Pirbadian, S.; Barchinger, S. E.; Leung, K. M.; Byun, H. S.; Jangir, Y.; Bouhenni, R. A.; Reed, S. B.; Romine, M. F.; Saffarini, D. A.; Shi, L.; Gorby, Y. A.; Golbeck, J. H.; El-Naggar, M. Y. *Shewanella oneidensis* MR-1 nanowires are outer membrane and periplasmic extensions of the extracellular electron transport components. *Proc. Natl. Acad. Sci. U. S. A.* **2014**, *111*, 12883−12888.
(50) Perez-Cruz, C.; Carrion, O.; Delgado, L.; Martinez, G.; Lopez-Iglesias, C.; Mercade, E. New type of outer membrane vesicle produced by the Gram-negative bacterium *Shewanella vesiculosa* M7(T): Implications for DNA content. *Appl. Environ. Microbiol.* **2013**, *79*, 1874−1881.
(51) Schwechheimer, C.; Kuehn, M. J. Outer-membrane vesicles from Gram-negative bacteria: biogenesis and functions. *Nat. Rev. Microbiol.* **2015**, *13*, 605−619.
(52) Hiemenz, P.; Rajagopalan, R. Electrophoresis and Other Electrokinetic Phenomena. *Principles of Colloid and Surface Chemistry*; CRC Press: Boca Raton, FL, 1977; Vol. *3*, pp 544−547.
(53) Hunter, R. J. *Zeta Potential in Colloid Science: Principles and Applications*; Academic Press: 2013.
(54) Feick, J. D.; Velegol, D. Electrophoresis of spheroidal particles having a random distribution of zeta potential. *Langmuir* **2000**, *16*, 10315−10321.
(55) Feick, J. D.; Velegol, D. Measurements of charge nonuniformity on polystyrene latex particles. *Langmuir* **2002**, *18*, 3454−3458.
(56) Blum, F. D. Magnetic resonance of polymers at surfaces. *Colloids Surf.* **1990**, *45*, 361−376.
(57) Claesson, P. M.; Dahlgren, M. A.; Eriksson, L. Forces between polyelectrolyte-coated surfaces: relations between surface interaction and floc properties. *Colloids Surf., A* **1994**, *93*, 293−303.
(58) Cosgrove, T.; Griffiths, P.; Lloyd, P. Polymer adsorption. The effect of the relative sizes of polymer and particle. *Langmuir* **1995**, *11*, 1457−1463.
(59) Lin, W.-Y.; Blum, F. D. Segmental dynamics of bulk and silica-adsorbed poly (methyl acrylate)-d_3 by deuterium NMR: the effect of molecular weight. *Macromolecules* **1998**, *31*, 4135−4142.
(60) Hershkovits, E.; Tannenbaum, A.; Tannenbaum, R. Polymer adsorption on curved surfaces: a geometric approach. *J. Phys. Chem. C* **2007**, *111*, 12369−12375.
(61) Blum, F. D.; Xu, G.; Liang, M.; Wade, C. G. Dynamics of Poly (vinyl acetate) in Bulk and on Silica. *Macromolecules* **1996**, *29*, 8740−8745.

https://dx.doi.org/10.1021/jacs.0c02737
J. Am. Chem. Soc. 2020, 142, 10814−10823